A Modular Multilevel Interface for Transformer-less Grid Integration of Large-Scale Infrastructure for Wireless Electric Vehicle Charging

Giuseppe Guidi[1], Salvatore D'Arco[1], Jon Are Suul[1,2], Ryosuke Iso[3], Jun-Ichi Itoh[3]

[1] SINTEF Energy Research, 7465 Trondheim, Norway
[2] Department of Engineering Cybernetics, Norwegian University of Science and Technology, 7495 Trondheim, Norway
[3] Dept. of Electrical, Electronics and Information Engineering, Nagaoka University of Technology, Nagaoka, Japan

***Abstract*-- This paper presents a system configuration for transformer-less grid integration of large-scale charging infrastructures for electric vehicles (EVs) with wireless inductive charging. The proposed configuration relies on a Modular Multilevel Converter (MMC) topology as the grid interface of the charging infrastructure, where one wireless EV charger can be supplied from each individual module. This system topology could provide significant reduction in footprint and complexity of cable installations by allowing for transformer-less connection and direct integration with the medium voltage distribution grid. The requirements for power flow management when charging EVs that are unevenly distributed within the infrastructure are evaluated analytically. On this basis, a control strategy is presented for ensuring horizontal and vertical energy balancing among the MMC arms, and voltage balancing among the modules of each arm. Time-domain simulations demonstrate how the system can operate with severe unbalances resulting from different number and location of charging EVs.**

***Index Terms*—Electric Vehicle Charging Infrastructure, Modular Multilevel Converters, Transformer-less Grid Interface, Wireless Power Transfer.**

I. Introduction

The increasing number of electric vehicles (EVs) concentrating in space-constrained urban areas is driving a need for development of large-scale EV charging facilities [1]. Infrastructures capable of simultaneously charging a high number of EVs are expected to require high-power installations in the multi-megawatt range [2], [3]. Moreover, compact solutions will become critical for large residential garages where tens or even hundreds of cars could be parked for being charged.

Wireless charging of EVs based on Inductive Power Transfer (IPT) technology is gaining acceptance as a preferred solution in terms of user convenience and is recognized as an enabling technology for future self-driving and autonomous vehicles [4],[5]. In such systems, the sending-side coil, which is usually supplied by a low voltage resonant converter, can be part of the fixed electrical infrastructure, while the receiving-side coil can be mounted on or integrated in the chassis of the vehicle [6]. Thus, wireless IPT-based charging systems provide inherent galvanic isolation between the vehicle and the power conversion system on the infrastructure side.

This paper proposes a system configuration for a large-scale EV charging infrastructure where the grid-side interface is based on a modular multilevel converter (MMC) topology [7]. In this topology, a wireless EV charger can be integrated in each individual module of the grid interface converter. The only required adaptation of the EV charger is that the sending-side systems must be designed to operate at a floating electrical potential defined by the operation of the MMC topology. This will not influence the vehicle-side system, and the voltage rating for the grid interface can be easily scaled by the number of modules in each phase of the MMC. Thus, the proposed configuration combines the unique features of MMC topologies with the inherent galvanic isolation provided by wireless charging. Since the MMC topology enables direct transformer-less integration with the medium voltage (MV) distribution grid, it could significantly reduce the space requirements and cabling complexity compared to a conventional design of a large-scale charging infrastructure with multiple transformers and a complex cabling network.

The proposed system configuration is partly inspired by previous studies of modular converter topologies utilized for grid integration of energy storage systems with low voltage battery modules at floating potential [9], [8]. The possibility of introducing power sources or loads in each module of modular converters has also been studied for solid-state transformers (SSTs) [10]-[12]. Furthermore, similar system configurations as in modular SSTs with high frequency transformers for galvanic isolation have been recently proposed to obtain modular systems for inductive power transfer, as discussed in [13]-[15]. However, most of these studied applications have a controllable or smoothly distributed loading of the module within the arms. However, for the application proposed in this paper, an arbitrary number of the modules in each arm of the converter can be fully loaded,

This work was supported by the project Modular Megawatt-range Wireless EV Charging Infrastructure Providing Smart Grid Services (MoMeWeC), funded by the Research Council of Norway under the EIG CONCERT Japan program, Joint Call on Efficient Energy Storage and Distribution, with project number 284231

This is the accepted version of a paper published at 2019 10th International Conference on Power Electronics and ECCE Asia - ICPE 2019 - ECCE Asia
ISBN: 978-89-5708-313-0

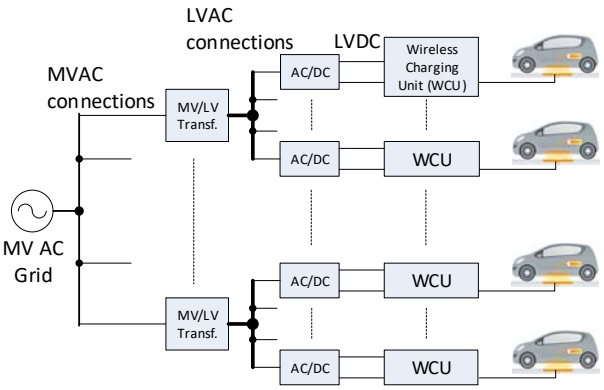

Fig. 1. Conventional connection layout for large parking infrastructure with (wireless) EV charging

disconnected or operating on partial load, depending on the presence and charging needs of the EVs. This implies additional challenges for the balancing of the capacitor voltages within each arm as well as between all the arms compared to applications for ac-dc power conversion or applications with a more evenly distributed load on all modules.

In this paper, the balancing requirements of the proposed MMC-based grid interface is analyzed and a control strategy for operating the topology in the full range of possible loading conditions is introduced. Simulation results are presented to demonstrate how the converter can be controlled to maintain balanced three-phase currents in the ac-distribution system while operating with generic unbalanced loading.

II. Proposed Charging Station Topology

Present high-power charging infrastructures are installed according to a conventional connection layout with parallel connection of low voltage charging units. In such configurations, a group of chargers (either wireless or conventional) are supplied by an internal low voltage (LV) bus, with a dedicated transformer for connection to the MV distribution system. The number of charging units that can be parallel-connected in each group is limited by the capacity of the low-voltage bus and by the rating of the MV/LV transformer. A typical configuration of a large-scale charging facility with a conventional distribution system is indicated in Fig. 1 for the case of wireless charging units (WCUs). The main drawbacks of this conventional layout are associated to the dimensioning of low voltage ac-buses for high currents, resulting in heavy and expensive cabling, together with the need for multiple MV/LV distribution transformers.

The proposed system configuration for large-scale wireless EV charging infrastructure is presented in Fig. 2. As can be seen from the figure, the topology is based on utilization of the MMC topology from [7] as a grid interface. Each phase of the grid-side interface consists of two arms that are connected between the phase and the upper or lower star-point. Thus, according to the terminology introduced in [16], the proposed topology is a double-star modular multilevel cascaded converter, where each sub-module capacitor is supplying the input

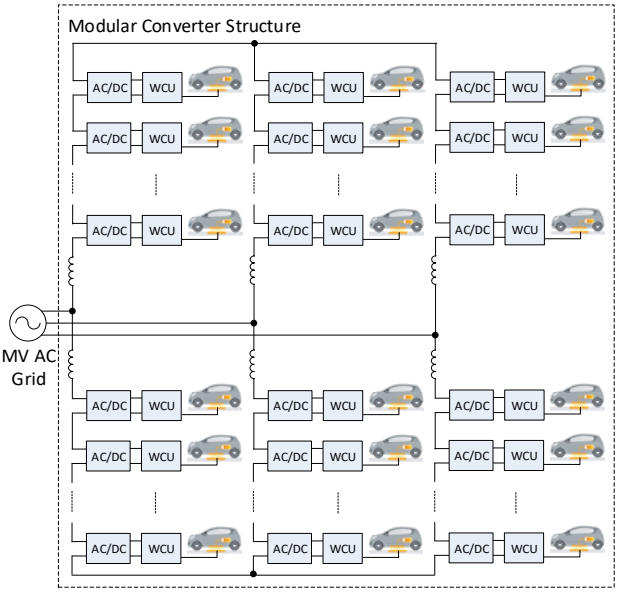

Fig. 2. Proposed connection layout of large parking infrastructure for wireless EV charging with MMC-based grid interface

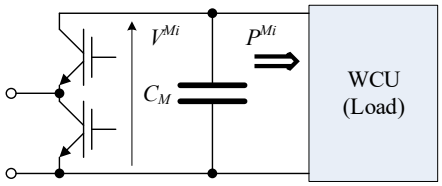

Fig. 3. Generic model of a parking spot with a WCU supplied by a module of the MMC-based grid interface converter

voltage to a WCU. This configuration results in a series connection of the charging units in each arm, where each WCU is supplied with a low voltage input at floating potential. The model of a charging point with a generic WCU load, supplied by a corresponding half-bridge module of the MMC topology, is presented in Fig. 3. Due to the modular structure, the system configuration is easily scalable, and the number of charging points connected in series within one arm can be selected according to the available MV grid and the desired scale of the charging infrastructure. The sum of the capacitor voltages of all modules in one arm should always be higher than the peak phase-to-phase voltage of the ac grid, while higher total capacitor voltage will allow for redundancy in the system.

The proposed configuration offers several advantages compared to the conventional charging infrastructure layout from Fig. 1, that can be summarized as:

i. The series connection of WCUs within the arms of the MMC-based topology allows for a high voltage rating of the grid-side interface and possibly a transformer-less connection directly to the MV grid. For large-scale charging infrastructures, this can allow to save the costs and the volume of multiple MV/LV transformers.
ii. The MMC-based topology is characterized by a low voltage THD at the ac-terminals compared to 2 level and 3 level converters, which will limit the requirements for ac output filters. This also translates in reduced costs and volume.

This is the accepted version of a paper published at 2019 10th International Conference on Power Electronics and ECCE Asia - ICPE 2019 - ECCE Asia
ISBN: 978-89-5708-313-0

iii. The grid connection at higher voltage levels and the series connection of the WCUs would simplify the cabling layout and reduce the cable lengths and cross sections. Within each arm, only direct series connection by a single-core cable is needed, with current capability defined by the voltage and power rating of an individual WCU.

The main disadvantage of the proposed topology will be the increased complexity in the control of the grid side interface, as will be discussed in the following, and the insulation requirements resulting from the series connected configuration. While it will be shown that the input capacitor voltage on each WCU from the corresponding module can be maintained almost constant, the voltage to ground will vary continuously with the operation of the converter. Indeed, the WCUs on the extremes of the series connection in each arm will experience the minimum and the maximum voltages. This should be accounted for when designing the insulation to ground for the WCUs. However, the combination of the MMC-based configuration and the wireless charging exploits the inherent benefit of IPT technology to ensure galvanic insulations from the EVs to be charged. Indeed, all parts of the system that will be exposed to the full voltage range of the MV grid can be integrated and encapsulated within the infrastructure, while no extra design measures will be needed for the equipment on the vehicles. Thus, users of the vehicles or the general public around the charging infrastructure will not be exposed to the increased voltage levels of the charging infrastructure, and the functionality for a user will be the same as for a WCU supplied by a conventional layout according to Fig. 1.

III. Definition of Variables and Per-Unit System

The system configuration introduced in Fig. 2 has the same general ac-side interface as the double star MMC topology commonly studied for HVDC transmission systems [16]. Thus, it is convenient to express the internal dynamics in terms of circulating currents [17].

In the following, a per-unit system is applied with base values derived from the total three-phase power rating, P_{nom}, the rated peak value of the grid-side phase voltage $V_{ph,nom}$, and the equivalent dc voltage that represents the limits for controllability of the converter (i.e. $V_{dc,nom} = \sqrt{3}\, V_{ph,nom}$). Using lower case symbols to represent per-unit quantities, the main variables of the MMC-based topology are defined by the following expressions:

$$i_x^{\Delta} = i_{x,u} - i_{x,l}, \qquad i_x^{\Sigma} = \frac{i_{x,u} + i_{x,l}}{2}, \qquad x \in abc \tag{1}$$

$$v_{x,y}^{\sigma} = \sum_{i=1}^{N} v_{x,y}^{M_i}, \qquad v_{x,y} \approx n_{x,y} \cdot v_{x,y}^{\sigma}, \quad x \in a,b,c \quad y \in u,l \tag{2}$$

$$c_{eq} \dot{v}_{x,y}^{\sigma} \approx n_{x,y} i_{x,y}, \qquad c_{eq} = C_M / N \tag{3}$$

$$v_x^{\sigma\Sigma} = v_{x,u}^{\sigma} + v_{x,l}^{\sigma}, \qquad v_x^{\sigma\Delta} = v_{x,u}^{\sigma} - v_{x,l}^{\sigma} \tag{4}$$

$$v_x^{\Delta} = \frac{v_{x,l} - v_{x,u}}{2} \approx \frac{n_{x,l} \cdot v_{x,l}^{\sigma} - n_{x,u} \cdot v_{x,u}^{\sigma}}{2} \tag{5}$$

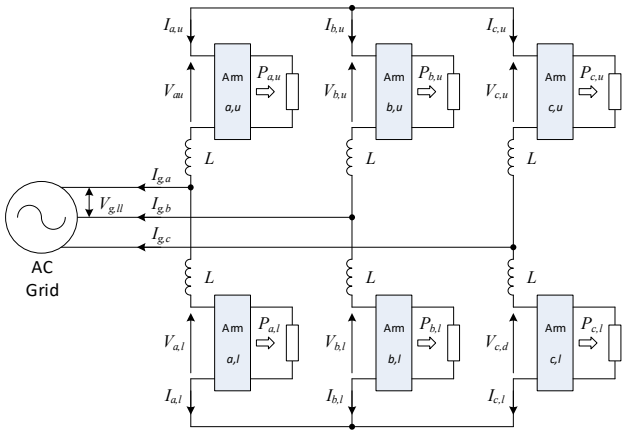

Fig. 4. Averaged Arm Model of double-star MMC converter with individually-loaded arms.

$$v_x^{\Sigma} = \frac{v_{x,l} + v_{x,u}}{2} \approx \frac{n_{x,l} \cdot v_{x,l}^{\sigma} + n_{x,u} \cdot v_{x,u}^{\sigma}}{2} \tag{6}$$

In these equations, the subscripts u and l refer to the upper and lower arms, respectively, while the superscripts Σ and Δ refer to the sum and difference between upper and lower arm quantities. Consequently, the grid-side current is represented by i_x^{Δ} while i_x^{Σ} represents the circulating current. The total available voltage in an arm, given by the sum of the capacitor voltages in the N modules, is represented by $v^{\sigma}_{x,y}$ according to (2), while $v_{x,y}$ represents the controlled output voltage from an arm. The insertion index $n_{x,y}$ of each arm is a signal between 0 and 1, which is defined to determine the relative share of the total available capacitor voltage $v^{\sigma}_{x,y}$ that is provided by the arm. The dynamics of the total arm voltage is given by (3), as a function of the arm current and the corresponding insertion index. The sum and difference of the total capacitor voltages in the upper and lower arms is defined in (4) by $v_x^{\sigma\Sigma}$ and $v_x^{\sigma\Delta}$, respectively. Finally, the arm voltage difference v_x^{Δ}, which is the equivalent voltage driving the grid-side currents, and the arm voltage sum, v_x^{Σ}, which will drive the circulating currents, are defined by (5) and (6), respectively.

A simplified illustration of the topology, by applying an averaged arm representation as shown in Fig. 4, is useful for evaluating the power flow balancing requirements between the different phases and arms of the converter topology. This figure, also shows how the total power flow in one arm, $P_{x,y}$, can be represented as an aggregated load on the equivalent dc-side capacitor of the averaged arm model when studying the power balancing between the arms.

Neglecting losses, the total per unit active power drawn from the grid equals the sum of all arm loads:

$$p_{tot} = \frac{1}{6} \sum_{\substack{x=a,b,c \\ y=u,l}} p_{x,y} = \sum_{\substack{x=a,b,c \\ y=u,l}} \left(\frac{1}{N} \sum_{i=1}^{N} p_{x,y}^{M_i} \right) \tag{7}$$

The horizontal unbalance between the phases can be quantified by subtracting the average phase power from the power absorbed in each phase:

$$p_x^{\Sigma'} = \frac{p_{x,u} + p_{x,l}}{2} - p_{tot} \tag{8}$$

This is the accepted version of a paper published at 2019 10th International Conference on Power Electronics and ECCE Asia - ICPE 2019 - ECCE Asia
ISBN: 978-89-5708-313-0

The vertical unbalance for each phase can be quantified as the difference between upper and lower arm power:

$$p_x^{\Delta} = \frac{p_{x,u} - p_{x,l}}{2} \tag{9}$$

IV. MMC Power Flow Requirements

In the proposed configuration for large-scale EV charging infrastructures, each individual wireless charging unit will drain power directly from a module of the MMC-based grid interface. Thus, the loading of the individual modules will depend on the location and power demand of the EVs to be charged. Since it is not likely that all charging units will be in operation at the same time, significant unbalance in the loading between the phases and within each phase of the topology must be expected. Therefore, the control system must be specifically designed to ensure internal balancing of the power flow and the capacitor voltages even in case of extreme unbalances in the loading, while still ensuring balanced three-phase currents at the interface with the grid. The following basic principles should be considered for operating the MMC-based parking infrastructure:

i. Sinusoidal and symmetrical grid current, i_x^{Δ}, should be imposed with magnitude and phase angle calculated to achieve overall active power balance and reactive power control for the grid interface.
ii. Compensation of horizontal load unbalance $p_x^{\Sigma'}$ between the phases can be ensured by the dc component of the circulating current [19], [20].
iii. Compensation of vertical load unbalance between upper and lower arms in each phase, p_x^{Δ} can be ensured with the fundamental frequency component of the circulating current [19], [20].
iv. Power balance between the modules of a given arm is achieved by conventional sorting algorithm for voltage balancing in the modulation of the output voltage. However, a minimum arm current is needed to ensure capacitor voltage balancing among modules with different loading. This can be achieved by introducing a 2nd harmonic component circulating current with magnitude related to the amount of power to be balanced.

The first point above immediately translates into an expression for the grid-side current as function of the grid voltage (assumed sinusoidal and symmetrical) and the total power:

$$\begin{cases} i_a^{\Delta} = -\dfrac{p_{tot}}{|v_g|} + j \cdot \dfrac{q_{tot}}{|v_g|} \\ i_b^{\Delta} = i_a^{\Delta} \cdot \alpha^2 \\ i_c^{\Delta} = i_a^{\Delta} \cdot \alpha \end{cases} \qquad \alpha = e^{j2\pi/3} \tag{10}$$

The other points above dictate that the circulating current will be the sum of several harmonic components:

$$i_x^{\Sigma} = i_{x,dc}^{\Sigma} + \mathrm{Re}\left(i_{x,\omega}^{\Sigma} \cdot e^{j\omega t}\right) + \mathrm{Re}\left(i_{x,2\omega}^{\Sigma} \cdot e^{j2\omega t}\right) \tag{11}$$

Each of these harmonic components are calculated in the following as function of the magnitude and distribution of the charging power.

A. DC current for horizontal power balancing

The average power over one fundamental period that is transferred to the two arms in one phase by a dc-component in the circulating current is evaluated as:

$$p_{x,dc} = 2 \cdot \sqrt{3} \cdot v_{dc} \cdot i_{x,dc}^{\Sigma} \tag{12}$$

The circulating dc current needed to counteract the horizontal unbalance defined in (8) is therefore calculated as:

$$i_{x,dc}^{\Sigma} = -\frac{1}{2 \cdot \sqrt{3}} \cdot \frac{p_x^{\Sigma'}}{v_{dc}} \tag{13}$$

It is noted that, by construction, the sum of all dc currents is zero, which is a necessary condition for a circulating current.

B. First harmonic current for vertical power balancing

The fundamental frequency component of the six arm currents must satisfy the following set of linear phasor equations, resulting from basic circuit considerations:

$$\begin{cases} v_{x,u,\omega} + v_{x,l,\omega} + j \cdot 2 \cdot x_L \cdot i_{x,\omega}^{\Sigma} = 0 \\ v_{x,l,\omega} + j \cdot x_L \cdot \left(i_{x,\omega}^{\Sigma} - \dfrac{i_{x,\omega}^{\Delta}}{2} \right) = v_{g,x,\omega} \end{cases} \tag{14}$$

The equations in (14) can be rewritten in terms of positive and negative sequence current components, considering that i_x^{Δ} and v_g contain only positive sequence components and that the circulating current contains only positive and negative sequence components:

$$\begin{cases} v_{a,u,\omega} + v_{a,l,\omega} + j \cdot 2 \cdot x_L \cdot \left(i_{+,\omega}^{\Sigma} + i_{-,\omega}^{\Sigma} \right) = 0 \\ v_{b,u,\omega} + v_{b,l,\omega} + j \cdot 2 \cdot x_L \cdot \left(\alpha^2 i_{+,\omega}^{\Sigma} + \alpha i_{-,\omega}^{\Sigma} \right) = 0 \\ v_{c,u,\omega} + v_{c,l,\omega} + j \cdot 2 \cdot x_L \cdot \left(\alpha i_{+,\omega}^{\Sigma} + \alpha^2 i_{-,\omega}^{\Sigma} \right) = 0 \\ v_{a,l,\omega} + j \cdot x_L \cdot \left(i_{+,\omega}^{\Sigma} + i_{-,\omega}^{\Sigma} - \dfrac{i_{+,\omega}^{\Delta}}{2} \right) = v_g \\ v_{b,l,\omega} + j \cdot x_L \cdot \left(\alpha^2 i_{+,\omega}^{\Sigma} + \alpha i_{-,\omega}^{\Sigma} - \alpha \dfrac{i_{+,\omega}^{\Delta}}{2} \right) = \alpha^2 v_g \\ v_{c,l,\omega} + j \cdot x_L \cdot \left(\alpha i_{+,\omega}^{\Sigma} + \alpha^2 i_{-,\omega}^{\Sigma} - \alpha^2 \dfrac{i_{+,\omega}^{\Delta}}{2} \right) = \alpha v_g \end{cases} \tag{15}$$

From this set of equations, expressions for the individual arm voltages can be found. Then for each arm, the total power $p_{x,y}$ must correspond to $\mathrm{Re}(v_{x,y,\omega} \cdot \mathrm{Conj}(i_{x,y,\omega}))$. Resolving the resulting expression results in the following expressions for the vertical power unbalances:

$$\begin{cases} p_a^{\Delta} = v_g \cdot \left(-\mathrm{Re}(i_{+,\omega}^{\Sigma}) - \mathrm{Re}(i_{-,\omega}^{\Sigma}) \right) \\ p_b^{\Delta} = v_g \cdot \left(-\mathrm{Re}(i_{+,\omega}^{\Sigma}) + \dfrac{1}{2}\mathrm{Re}(i_{-,\omega}^{\Sigma}) - \dfrac{\sqrt{3}}{2} \cdot \mathrm{Im}(i_{-,\omega}^{\Sigma}) \right) \\ p_c^{\Delta} = v_g \cdot \left(-\mathrm{Re}(i_{+,\omega}^{\Sigma}) + \dfrac{1}{2}\mathrm{Re}(i_{-,\omega}^{\Sigma}) + \dfrac{\sqrt{3}}{2} \cdot \mathrm{Im}(i_{-,\omega}^{\Sigma}) \right) \end{cases} \tag{16}$$

It is noted that the imaginary part of the positive sequence component plays no part in the vertical balancing process. Equivalently to what was originally presented in [18],

This is the accepted version of a paper published at 2019 10th International Conference on Power Electronics and ECCE Asia - ICPE 2019 - ECCE Asia
ISBN: 978-89-5708-313-0

solving the equation above reveals that a complete set of independent control variables for vertical balancing of an MMC can be obtained by the following components:

$$\begin{cases} \mathrm{Re}(i^{\Sigma}_{+,\omega}) = -\dfrac{p^{\Delta}_{a,\omega} + p^{\Delta}_{b,\omega} + p^{\Delta}_{c,\omega}}{3 \cdot v_g} \\ \mathrm{Re}\left(i^{\Sigma}_{-,\omega}\right) = -\dfrac{2 \cdot p^{\Delta}_{a,\omega} - p^{\Delta}_{b,\omega} - p^{\Delta}_{c,\omega}}{3 \cdot v_g} \\ \mathrm{Im}\left(i^{\Sigma}_{-,\omega}\right) = -j\dfrac{\sqrt{3} \cdot p^{\Delta}_{b,\omega} - \sqrt{3} \cdot p^{\Delta}_{c,\omega}}{3 \cdot v_g} \end{cases} \quad (17)$$

This equation shows that the real part of the fundamental frequency positive sequence circulating current is associated with the overall imbalance between upper and lower arms, while the imaginary part can be chosen freely without violating the power balance. However, selecting the imaginary part to be zero will minimize the total rms value of the arm currents, due to the orthogonality of the components. The equation also shows that the negative sequence of the circulating current balances upper and lower arm power of individual arms. The real part causes the vertical imbalance of phase *a* to change in opposite direction from the one of the other two phases, while the imaginary part causes the vertical imbalance of phase *b* to change in opposite direction from phase *c*, leaving the vertical imbalance of phase *a* unchanged.

C. Intra-arm balancing

Once the six aggregated arms in Fig. 4 are balanced by the dc and fundamental frequency circulating current components calculated in the previous subsections, the problem of internal capacitor voltage balancing within each arm still remains. However, moving energy between cells within one arm can only be achieved by properly selecting the cells to generate the necessary arm output voltage, with a similar process as the sorting algorithms used in conventional MMC control [7]. It must also be considered that there are some theoretical limits for the balancing capabilities, depending on the magnitude and shape of the arm currents.

Let $P^{M}_{\max}$ be the highest load within a given arm:

$$P^{M}_{\max} = \max_{i=1,..,N}\left(P^{M_i}\right) \quad (18)$$

Assuming the load to be constant over the fundamental period, and that no energy is fed from the arm into one loaded module (see Fig. 3), the dc-link voltage will be discharged as given by:

$$\Delta V^{M}_{\max} = \frac{1}{C_M} \cdot \int_0^T \frac{P^{M}_{\max}}{V^{M}} \cdot dt \approx \frac{T}{C_M} \cdot I^{M} \quad (19)$$

To keep V^{M} stable over time, an equal amount of energy must be supplied to the module by the arm current. According to the polarity shown in Fig. 4, positive arm current counteracts the discharging effect of the cell load. Therefore, a necessary condition for cell voltage stability is:

$$\int_0^T I'_x(t) \cdot dt \geq I^{M} \cdot T \quad (20)$$

where I_x' is the positive part of the arm current I_x:

$$I'_x(t) = \max\{I_x(t), 0\}$$

If the arm current flowing due to power balancing between the arms does not satisfy (20), stable capacitor voltages within the arm cannot be achieved without further control efforts. However, intra-arm power balancing capability can be improved by adding an even harmonic component (for instance 2nd harmonic) to the circulating current.

To reduce losses, it is desirable to insert the minimum possible 2nd harmonic current that allows for cell voltage balancing on all arms under the specific operating conditions. Solving the general problem of minimum 2nd harmonic insertion is beyond the scope of this paper. Instead, the simple but meaningful operating condition corresponding to only one cell loaded with its rated power is analyzed. Assuming a sufficiently high number of modules in the system, the condition corresponds to negligible total power and negligible inter-arm unbalance, leading to an arm current of pure 2nd harmonic. The necessary condition (20) is then easily calculated analytically and can be expressed in per unit values as:

$$\left|i^{\Sigma}_{2\omega}\right| \geq \frac{\pi}{4\sqrt{3}} \cdot \frac{1}{v^{\sigma}_x} \approx \frac{0.45}{v^{\sigma}_x} \quad (21)$$

Operating the system with voltage redundancy (i.e. $v^{\sigma}_x > 1$) reduces the need for additional 2nd harmonic current for balancing. Moreover, voltage redundancy also brings the necessary condition (20) closer to a sufficient one, since it increases the freedom of connecting the module only when the arm current has the desired polarity. It is noted that while the condition in (21) strictly applies only to a very special operating condition, it is expected to be close to the worst-case as far as intra-arm balancing is concerned.

V. Proposed Control Strategy

Based on the analysis in the previous section, a control system for operating the grid-side interface of the proposed MMC-based wireless charging infrastructure can be designed. As the total power and the internal power differences defined in the previous section are directly related to the corresponding capacitor voltages, as can be derived from (3), the arm power balancing can be based on control of the total arm capacitor voltages (or energies). The proposed control structure is shown in Fig. 5, and contains the following main loops for capacitor voltage control and power flow balancing:

i. An "Average Voltage Controller" which balances the total power flow to the MMC-based interface by providing the *d*-axis current reference i_d^{Δ} for control of the grid-side [21]. This control loop is a simple PI-controller operating on the zero-sequence component of the total capacitor voltages in all the three legs. By providing a *d*-axis current reference to a conventional *dq*-frame current controller, this control loop fulfills the requirements from (10).
ii. A "Voltage Sum Controller" which regulates the average value of $v_x^{\sigma\Sigma}$ for all the three legs to a reference value. The control loop for each phase is a

This is the accepted version of a paper published at 2019 10th International Conference on Power Electronics and ECCE Asia - ICPE 2019 - ECCE Asia
ISBN: 978-89-5708-313-0

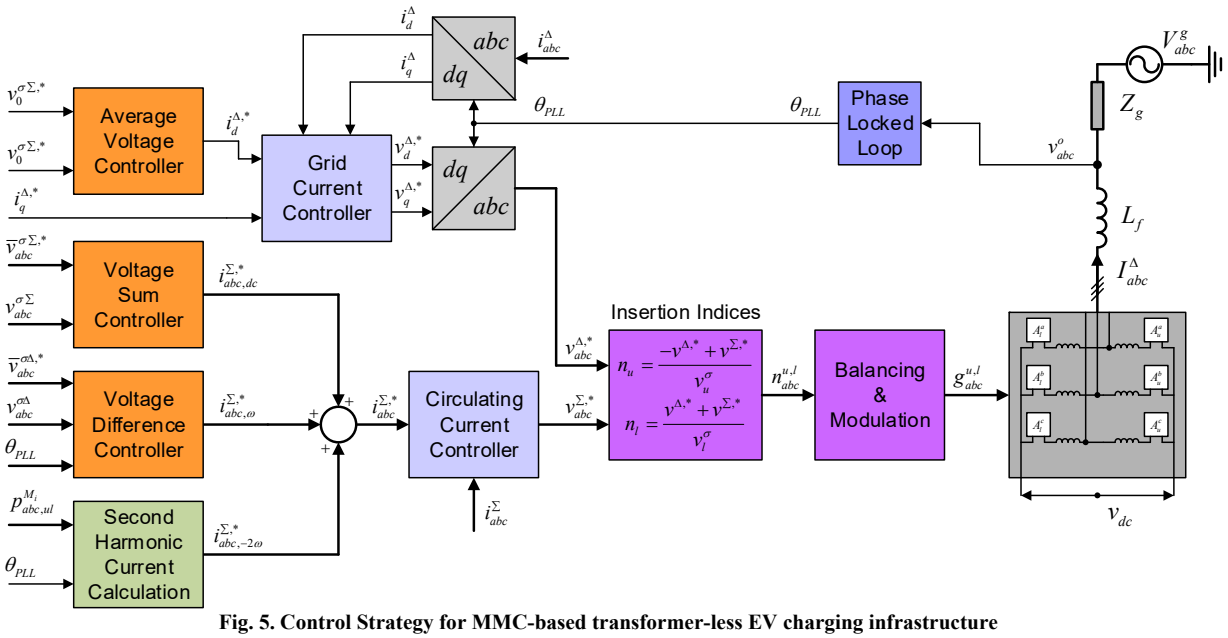

Fig. 5. Control Strategy for MMC-based transformer-less EV charging infrastructure

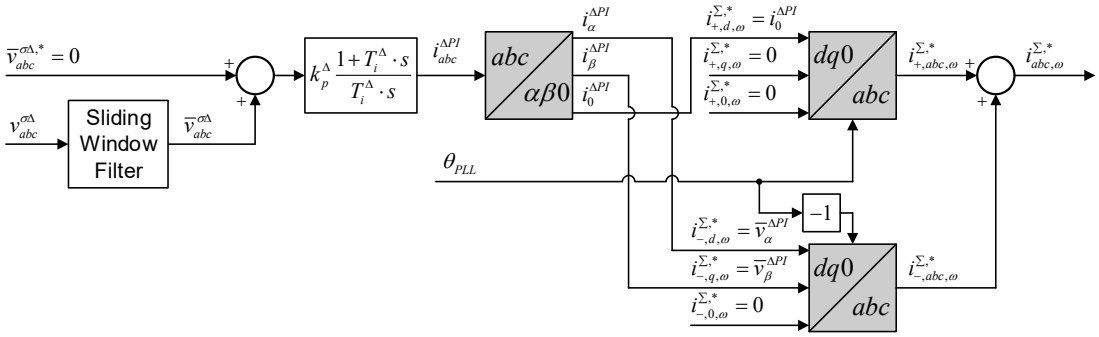

Fig. 6. Control loop for regulating the arm voltage differences to zero

simple PI-controller providing the dc-component of the circulating current, but a filter is required in the feedback signal to extract the dc component of the total capacitor voltage. By controlling $v_x^{\sigma\Sigma}$ to a fixed reference value, this control loop eliminates any horizontal voltage unbalances associated with $p_x^{\Sigma'}$ and ensures that (13) is satisfied in steady-state.

iii. A "Voltage Difference Controller" which regulates the average value of $v_x^{\sigma\Delta}$ to zero for all the three phases by controlling the fundamental frequency component of the circulating current. The implementation of the control loop is shown in Fig. 6, indicating how a sliding window filter is used to extract the average value of $v_x^{\sigma\Delta}$ before the resulting deviation is fed to a PI-controller for each phase. For the implementation, it is considered that (17) has the same form as the *abc* to *αβ0* transformation. Thus, the zero-sequence component of the output from the PI-controller, $i_0^{\Delta PI}$, is used to control the d-axis component of the positive sequence circulating current. Similarly, the *α*- and *β*-components of the controller output are used to control the *d*- and *q*-axis components (i.e. the real and imaginary parts) of the negative sequence circulating currents. Transforming these current components back to the stationary *abc*-frame and summing the positive and negative sequence components provides a set of current references that will fulfill the condition given by (17).

iv. An algorithm for estimating the required second harmonic circulating current $i^{\Sigma}_{abc,-2\omega}$ for ensuring that the condition in (20) is fulfilled.

For operating the presented control system, any conventional approach for control of the grid-side and circulating currents can be applied. Similarly, a conventional balancing and modulation algorithm according to the indications from [7] can be applied for operating the converter. However, it should be noted that the insertion index signals for each arm should be calculated by the equations given in Fig. 5, according to [17], to avoid that the arm voltage oscillations of the topology will have significant impact on the current control.

VI. Simulation Results

An example of a parking infrastructure characterized by the parameters in Table I has been investigated with a simulation model in Matlab/Simulink. Each charging spot has been modeled as a conventional half-bridge-based MMC-module with a constant-power load on the dc-side according to Fig. 3, and the modules are connected to form the double-star MMC topology of Fig. 2.

This is the accepted version of a paper published at 2019 10th International Conference on Power Electronics and ECCE Asia - ICPE 2019 - ECCE Asia
ISBN: 978-89-5708-313-0

TABLE I – PARAMETERS OF SIMULATED MODULAR CHARGING SYSTEM

System data	
Total installed charging power, P_{nom}	3.3 *MW*
Nominal line-to-line grid voltage, $V_{g,nom}$	11 *kV*
Number of charging spots	300 (6x60)
MMC general data	
MMC Topology	Double-star
Number of modules per arm, N	50
Virtual dc-link voltage (MMC arm voltage), $V_{dc,nom} = V^{\sigma}_{nom}$	30 kV
MMC cell data	
Nominal load for each module, $P^{M,nom}$	11 k*W*
Nominal module voltage, $V^{M,nom}$	600 *V*
Module capacitance, C_M	3.4 mF

TABLE III – SIMULATED LOAD DISTRIBUTION ON MMC ARMS

	a,u	***a,l***	***b,u***	***b,l***	***c,u***	***c,l***
N. of loaded modules	15	28	7	20	35	45
Load (pu)	0.30	0.56	0.14	0.40	0.70	0.90

TABLE III – HARMONIC CONTENT OF ARM CURRENTS IN PU (FROM FFT OF TIME-DOMAIN SIMULATION)

	a,u	***a,l***	***b,u***	***b,l***	***c,u***	***c,l***
dc	0.01		0.03		0.04	
Fundamental	0.18	0.31	0.18	0.31	0.20	0.29
2nd harmonic	0.29					

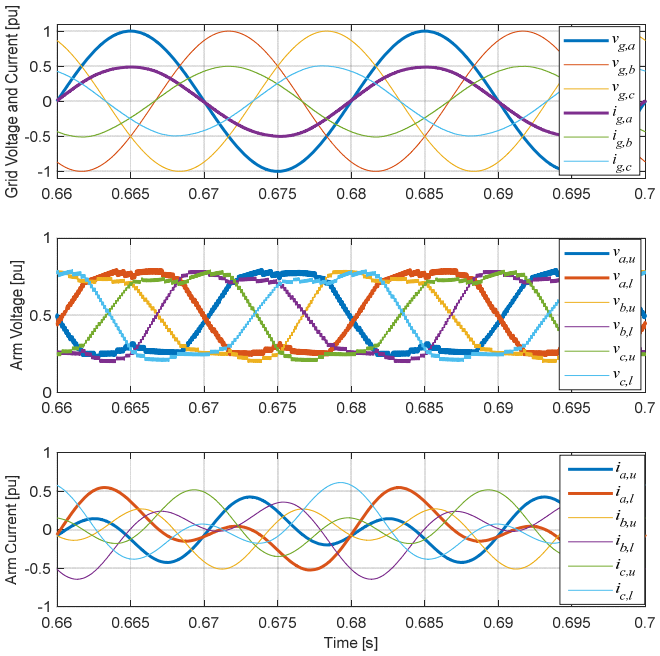

Fig. 7. Simulated operation of MMC-based transformer-less EV charging infrastructure, with curves showing (from top to bottom): i) Grid Voltage and current on the three phases (pu), ii) Voltages generated by each of the 6 MMC arms (pu), iii) Currents flowing in each of the 6 MMC arms (pu)

For assessing the feasibility of the proposed system configuration and to investigate potential issues related to unbalanced loading of individual modules, simulation results related to a typical condition are presented. Therefore, only a fraction of the available parking spots are assumed to be in operation. Moreover, the distribution of the loads is not balanced among the six arms of the converter. In the simulated case, half of the charging spots are active at rated power (11 kW), while the remaining spots are inactive, resulting in about 0.5 pu load seen from the grid. The load of the individual arms is indicated in Table II. Note that the simulated condition implies all the different kinds of load unbalances normally encountered in the proposed topology: i.e. horizontal, vertical and intra-arm unbalances. In the simulation, a balanced 2nd harmonic component of magnitude 0.3 pu is injected to the circulating current reference, to ensure intra-arm balancing. The value of this current component has been estimated from (21), with about 25% margin.

The upper plot in Fig. 7 shows the grid voltage and current expressed in per unit quantities. Despite the considerable internal unbalance, the MMC draws symmetrical currents from the grid with unity (controllable) power factor and negligible harmonic distortion, proving the effectiveness of the proposed control and modulation strategies. Moreover, due to the large number of MMC levels, the currents are essentially free of high frequency ripple. The middle and lower plots in Fig. 7 show the MMC arm voltages and currents. Dominant harmonic components of the arm currents, obtained by performing FFT on the simulation results, are also reported in Table III. It can be verified that the dc component and the fundamental frequency harmonic component correspond with very good accuracy to the theoretical values calculated using the analytical expression presented in the previous sections.

The upper plot in Fig. 8 shows the variation of the dc voltage of all the 300 modules in the system, showing that all voltages are bound within plus/minus 10% of their rated value. In particular, the second plot in Fig. 8 shows the dc voltage of one loaded and one unloaded module on arm *a,u*. The fact that the two voltages follow a very similar trajectory validate the proposed intra-arm balancing technique. The operation of the latter is made explicit in the lowest plots in Fig. 8, showing the power supplied to those two modules via the arm current. It is apparent that the loaded module participates in the synthesis of the arm voltage almost only when the arm current has positive polarity, so that the inflow of power is maximized. On the other hand, participation of the unloaded module is distributed over the whole time, resulting in zero net power intake.

VII. CONCLUSIONS

A system configuration for large-scale electric vehicle charging infrastructures has been presented. The proposed solution is based on series connection of charging spots, forming the double-star three-phase configuration often used in Modular Multilevel Converters (MMC). The topology is proposed for wireless inductive charging, taking advantage of the inherent galvanic isolation of such solutions, since the topology requires the modules to be operated at floating potential with respect to ground.

The presented system configuration has clear potential advantages compared to conventional topologies in terms of required length and cross section of cables. Moreover,

This is the accepted version of a paper published at 2019 10th International Conference on Power Electronics and ECCE Asia - ICPE 2019 - ECCE Asia
ISBN: 978-89-5708-313-0

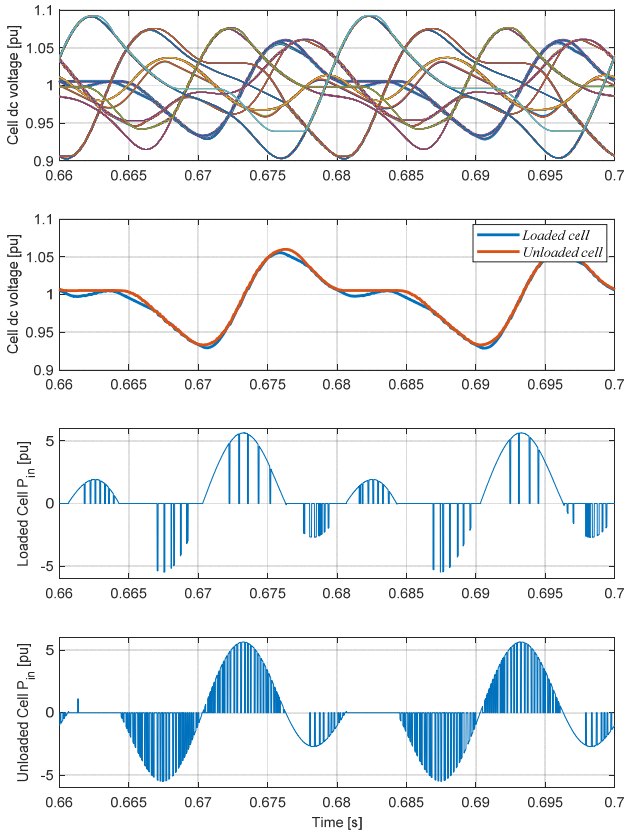

Fig. 8. Simulated operation of MMC-based transformer-less EV charging infrastructure, with curves showing (from top to bottom): i) Dc-link voltage of all 360 MMC cells (charging spots); ii) Dc-link voltage of one loaded and one unloaded cell within arm *a-u;* iii) Input power of the loaded cell; iv) Input power of the unloaded cell.

transformer-less connection to the distribution grid and reduced filtering requirements are made possible, with consequent savings in terms of footprint and cost.

The basic operating principles of the system have been analyzed, as basis for proposing a suitable control structure that has been validated by time-domain simulations. The requirements for internal power flow balancing have been analytically evaluated, forming the basis for future optimization of the control. Analysis has shown that although there are no theoretical limitations to the distribution of the EVs to be charged, the proposed topology may need rather high circulating currents to correctly convey the power flow from the grid to the individual modules. Future research efforts will be concentrated on finding optimum operating strategies and in clarifying the conditions in which the proposed topology is preferable over conventional solutions.

REFERENCES

[1] S. Chen, Y. Ji, L. Tong, "Large Scale Charging of Electric Vehicles," in *Proc. of the 2012 IEEE Power and Energy Society General Meeting*, San Diego, CA, USA, 22-26 July 2012, 8 pp.

[2] I. S Bayram, G. Michailidis, M. Devetsikiotis, "Electric Power Resource Provisioning for Large Scale Public EV Charging Facilities," in *Proc. of the 2013 IEEE International Conference on Smart Grid Communications*, Vancouver, Canada, October 2013

[3] I. S Bayram, A. Tajer, M. Abdallah, K. Qaraqe, "Capacity Planning Framework for Electric Vehicles Charging Stations With Multiclass Costumers" in *IEEE Transactions on Smar Grid*, Vol. 6, No. 4, July 2015, pp. 1934-1943

[4] G. Maggetto. P. Van den Bossche, "Inductive Automatic Charging: The Way to Safe, Efficient and User-Friendly Electric Vehicle Infrastructure, in *Proceedings of the 18th International Electric Vehicle Symposium and Exhibition*, EVS-18, Berlin, Germany, 20-24 October 2001, 12 pp.

[5] M. Kane, "Wireless Charging And Autonomous Electric Cars Go Hand-In Hand", InsideEVs, 09.04.2017, https://insideevs.com/wireless-charging-autonomous-electric-cars/

[6] S. Li and C. C. Mi, "Wireless power transfer for electric vehicle applications," *IEEE Journal of Emerging and Selected Topics in Power Electronics*, Vol. 3, No. 1, pp. 4–17, March 2015.

[7] A. Lesnicar, R. Marquart, "An Innovative Modular Multilevel Converter Topology Suitable for a Wide Power Range," *in Proceedings of the 2003 IEEE Bologna PowerTech*, 23-26 June 2003, Bologna, Italy, pp. 272-277

[8] N. Kawakami, S. Ota, H. Kon, S. Konno, H. Akagi, H. Kobayashi, N. Okada, "Development of a 500-kW Modular Multilevel Cascade Converter for Battery Energy Storage Systems," in *IEEE Transactions on Industry Applications*, Vol. 50, No. 6, pp. 3902-3910, November/December 2014

[9] D. Ronanki, S. S. Williamson, "Modular Multilevel Converters for Transportation Electrification: Challenges and Opportunities," in *IEEE Transactions on Transportation Electrification*, Vol. 4, No. 2, June 2018, pp. 399-407

[10] F. Briz, M. López, A. Rodríguez, M .Arias, "Modular Power Electronic Transformers – Modular Multilevel Converters Versus Cascaded H-Bridge Solutions," in *IEEE Industrial Electronics Magazine*, Vol. 10, No. 4, December 2016, pp. 6-19

[11] F. Briz, M. López, A. Zapico, A. Rodríguez, D. Diaz-Reigosa, "Operation and control of MMCs using cells with power transfer capability," in *Proceedings of the 30th Annual IEEE Applied Power Electronics Conference and Exposition*, APEC 2015, Charlotte, North Carolina, USA, 15-19 March 2015, pp. 980-987

[12] M. López, F. Briz, A. Zapico, A. Rodríguez, D. Diaz-Reigosa, "Control Strategies for MMC Using Cells with Power Transfer Capability" in *Proceedings of the 7th Annual IEEE Energy Covnersion Congress and Exposition*, ECCE 2015, Montreal, Quebec, Canada, 20-24 September 2015, pp. 3570-3577

[13] B. S. Riar, U. Madawala, "A Modular Multi-level Converter (M2LC) based on Inductive Power Transfer (IPT) Technology, in *Proceedings of the 3rd IEEE International Conference on Sustainable Energy Technologies*, ICSET 2012, Kathmandu, Nepal, 24-27 September 2012, pp. 54-59

[14] B. S. Riar, U. K. Madawala, D. J. Thrimawithana, "Analysis and Control of a Three-phase Modular Multi-level Converter based on Inductive Power Transfer Technology (M2LC-IPT)" in *Proceedings of the 2013 IEEE International Conference on Industrial Technology*, Cape Town, 25-28 February 2013

[15] K. Kandasamy, D. M. Vilathgamuwa, U. K. Madawala, K.-J. Tseng, "Inductively coupled modular battery system for electric vehicles," in *IET Power Electronics*, Vol. 9, No. 2, March 2016

[16] H. Akagi, "Classification, Terminology and Application of the Modular Multilevel Cascade Converter (MMCC)," in *IEEE Trans. on Power Electron.*, Vol. 26, No. 11, pp. 3119-3130, Nov 2011

[17] A. Antonopoulos, L. Ängquist, and H.-P. Nee, "On dynamics and voltage control of the modular multilevel converter," in *Proc. of the 13th European Conference on Power Electronics and Applications*, EPE'09, Barcelona, Spain, 8-10 September 2009, 10 pp.

[18] D. Soto-Sanchez, T. C. Green, "Control of a modular multilevel converter-based HVDC transmission system," in *Proc. of the 2011 14th European Conference on Power Electronics and Applications*, EPE 2011, Birmingham, UK

[19] T. Soong, P. W. Lehn, "Internal Power Flow of a Modular Multilevel Converter With Distributed Energy Resources," in *IEEE Journal of Emering and Selected Topics in Power Electronics*, Vol. 2, No. 4, pp. 1127-1138, December 2014

[20] H. Bayat, A. Yazdani, "A Power Mismatch Elimination Strategy for an MMC-based Photovoltaic System," in *IEEE Trans.on Energy Conv.*, Vol. 33, No. 3, pp. 1519-1528, September 2018

[21] G. Bergna, J. A. Suul, E. Berne, J.-C. Vannier, M. Molinas, "MMC Circulating Current Reference Calculation in ABC Frame by means of Lagrange Multipliers for Ensuring Constant DC Power under Unbalanced Grid Conditions," in *Proc. of the 16th Eur. Conf. on Power Electronics and Applications*, EPE'14 ECCE Europe, Lappeenranta, Finland, 26-28 August 2014

This is the accepted version of a paper published at 2019 10th International Conference on Power Electronics and ECCE Asia - ICPE 2019 - ECCE Asia
ISBN: 978-89-5708-313-0